Optimal Sizing of the Energy Storage System for Plug-in Fuel Cell Electric Vehicles, Balancing Costs, Emissions and Aging

Ahmad Eid El-Iali, Moustapha Doumiati, Mohamed Machmoum

Journal of Energy Storage 92 (2024) 112095

Contents lists available at ScienceDirect

Journal of Energy Storage

journal homepage: www.elsevier.com/locate/est

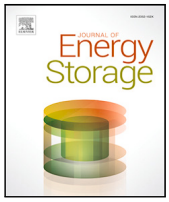

Research papers

Optimal sizing of the Energy Storage System for plug-in Fuel Cell Electric Vehicles, balancing costs, emissions and aging

Ahmad Eid El-Iali [a,b], Moustapha Doumiati [a,b,*], Mohamed Machmoum [a]

[a] IREENA Lab UR 4642, Nantes University, 37 bd de l'Université, Saint-Nazaire, 44600, France
[b] ESEO, 10 Bd Jeanneteau, Angers, 49100, France

ARTICLE INFO

Keywords:
Electric vehicle
Sizing optimization
Energy management optimization
Hybrid energy storage durability
CO2 emissions reduction

ABSTRACT

This research investigates the optimal sizing of the Energy Storage System (ESS) for Plug-in Fuel Cell Electric Vehicles (PFCEVs), taking into account technical, economic, and environmental challenges. The primary goal is to minimize both life cycle costs (LCC) and operational costs while simultaneously reducing CO2 emissions and preserving the durability of the power system. The PFCEV's ESS comprises three core components: a battery, a proton-exchange membrane fuel cell (FC) system, and a supercapacitor (SC). Performance evaluation involves strict constraints on the vehicle's operational parameters, and simulations are conducted following the Urban Dynamometer Driving Schedule (UDDS). A notable contribution of this research is the implementation of a double-loop optimization technique using quadratic programming (QP) and a genetic algorithm (GA) to identify a feasible solution space that respects the specified constraints. In summary, the findings yield valuable insights and recommendations for the optimal sizing of PFCEV ESS. The comparative analysis conducted between different PFCEVs, Fuel Cell Vehicles (FCVs), and Battery Electric Vehicles (BEVs), reveals that PFCEVs demonstrate distinct advantages. Finally, a sensitivity analysis concerning various hydrogen types shows a need for cost reduction in producing green hydrogen to improve its economic feasibility and operational efficiency.

1. Introduction

1.1. Context and motivation

Climate change poses a significant challenge for humanity, and the transportation sector plays a substantial role in the emission of greenhouse gases. According to the International Energy Agency in 2020, approximately 23% of global energy-related carbon dioxide (CO2) emissions were attributed to transportation [1]. The primary source of emissions from this sector is the combustion of fossil fuels, particularly gasoline and diesel, which power the majority of vehicles worldwide. When these fuels are burned, they release CO2 into the atmosphere. This contributes to the accumulation of greenhouse gases, which are responsible for global warming and the resulting climate change.

Recent technological advancements and growing environmental concerns have driven the electrification of the transportation sector, including passenger vehicles, trains, aircrafts, and more. This shift toward electrification signifies a substantial transition to a more sustainable and environmentally friendly mobility system. In terms of reducing CO2 emissions in transportation, lithium-ion batteries are one of the most prevalent technologies and are favored for their high energy density and long cycle life. Fuel cells (FCs) offer a compelling solution for electrifying powertrains in electric vehicles (EVs) and diverse transportation sectors like trains [2], ferries [3], and aircrafts [4–6]. These power sources present a clean energy alternative by transforming chemical energy into electricity.

The Energy Storage System (ESS) stands as a vital component within innovative electric powertrain transportation systems, significantly influencing their weight, performance and driving range. This is particularly important for aircraft systems as they need to meet certain volume and mass constraints [5,7], as well as EVs [8,9]. To enhance the system's range and make it more practical for daily use, it is important to correctly size its powertrain. The component sizing decides the potentials (e.g. dynamics, economy, and cost) of the powertrain and the effectiveness of the on-board energy management since it is necessary to have an on-board energy management system (EMS) that is well-designed to reduce component stress and extend their lifespan in addition to maximizing overall efficiency [10]. ESS significantly affects the vehicle performance, fuel economy, and emission performance. If a system has an oversized battery pack or ESS, it can lead to unnecessary extra weight and increased cost, which affects overall efficiency. On the other hand, if the ESS is undersized, it may limit the range and

* Corresponding author at: IREENA Lab UR 4642, Nantes University, 37 bd de l'Université, Saint-Nazaire, 44600, France.
E-mail address: moustapha.doumiati@eseo.fr (M. Doumiati).

https://doi.org/10.1016/j.est.2024.112095
Received 5 October 2023; Received in revised form 26 April 2024; Accepted 12 May 2024
Available online 24 May 2024

Abbreviations

BEV	Battery Electric Vehicle
CO2	Carbon Dioxide
EMS	Energy Management System
ESS	Energy Storage System
EV	Electric Vehicle
FC	Fuel Cell
FCV	Fuel Cell Vehicle
GA	Genetic Algorithm
HEV	Hybrid Electric Vehicle
LCC	Life Cycle Cost
LCE	Life Cycle Emissions
PFCEV	Plug-in Fuel Cell Electric Vehicle
QP	Quadratic Programming
SC	Super Capacitor
SoC	State of Charge
SoV	State of Voltage
UDDS	Urban Dynamometer Driving Schedule
WLTP	Worldwide Harmonized Light Vehicles Test Procedure

performance capabilities, compromising its durability. Consequently, component sizing and energy management are the two major factors that determine the costs (i.e. initial and operating costs) and the pollution contributions of the vehicle. To pursue low costs and emissions, these two aspects should be dealt with properly for cost-effective and environmentally friendly vehicles.

Ensuring the longevity of ESS is essential, particularly concerning the battery and the FC system, as they exhibit susceptibility to rapid aging when deviating from standard operating conditions, this includes disregarding dynamics, high power usage, and particularly deviating from standard temperature ranges. Research indicates that elevated temperatures beyond standard operating conditions accelerate the aging process and reduce the performance in both batteries [11,12] and FCs [13]. Consequently, effective thermal management becomes necessary to dissipate excess heat from these components, prolonging their lifespan, and improving overall efficiency [14]. Moreover, powertrains reliant on these energy sources encounter challenges such as cold starts in freezing climates following prolonged parking, which can result in failed starts and further degradation. Nonetheless, a recent innovation in thermal management proposes utilizing a vehicle-to-grid architecture to optimize the warm-up process of these on-board energy sources [15]. Another recent study [12] presents a review of different thermal management system strategies for an EV's battery.

With the different energy sources, different types of EVs offer distinct advantages and challenges. Battery electric vehicles (BEVs) have zero tailpipe emissions, lower operating costs, and higher energy efficiency compared to traditional internal combustion engine vehicles. However, they do face challenges such as higher initial costs, limited range, and lengthy charging times [16]. HEVs provide benefits such as improved fuel economy and lower emissions compared to traditional vehicles, and they lack the range limitations of BEVs. Nonetheless, HEVs are frequently more expensive than traditional vehicles and have less potential for emissions reduction compared to BEVs [17]. Fuel cell vehicles (FCVs) hold the potential for emissions-free driving by utilizing hydrogen and offer a longer driving range compared to BEVs, but they face challenges such as high initial costs, limited refueling infrastructure, and limited availability [18,19]. Each of these vehicle types offers unique advantages but also faces specific obstacles that need to be addressed for wider adoption and greater emissions reduction in the transportation sector.

The hybridization of the ESS can improve both range and performance while reducing overall weight [20]. For instance, Plug-in Fuel Cell Electric Vehicles (PFCEVs) represent a promising solution that merges the benefits of both BEVs and FCEVs. These vehicles rely on a dual energy system, combining a FC system (which uses stored hydrogen) and an externally charged battery as their main sources of energy. This combination allows PFCEVs to overcome the limitations experienced by both BEVs and FCEVs. Previous research has investigated various powertrain configurations within this architecture, including series, parallel and power split configurations [21]. Super Capacitors (SCs) are occasionally integrated into the energy storage system (ESS) of EVs due to their high power density [8,21–25]. Adding SCs to a PFCEV architecture offers a solution to alleviate battery and FC stress as they are able to quickly supply and absorb substantial amounts of power, making them well-suited to support primary energy sources during acceleration and braking phases. This combination leads to a prolonged ESS lifespan and enhanced efficiency for the EV.

1.2. Related works

ESS sizing methods can be classified into three categories: experience-based, calculation-based, and optimization-based [26]. Experience-based approaches draw on previous EV design databases or trial and error. Calculation-based methods employ mathematical equations to size the ESS according to specific power or range requirements. Optimization-based techniques, on the other hand, focus on finding the optimal sizing of EVs, PFCEVs, and other complex powertrains by formulating the objectives into a global cost function, which has been the focus of prior research. In [8], a model-based multi-objective optimization approach was employed to determine the optimal sizing of an ESS consisting of batteries and SCs. The optimization process considered factors such as system cost, system weight, and total battery degradation. To evaluate the battery's state of health, a wavelet-transform-based EMS was utilized to distribute power between the batteries and SCs. The Non-dominated Sorting Genetic Algorithm-II was employed to solve the optimization problem. Notably, the study did not take into account the operation cost, as the battery was considered the primary energy source in the EV. In [27], the optimal sizing of a PFCEV was investigated with a focus on minimizing both the system cost and the operation cost of the vehicle, since the considered EV utilized both a FC system and a battery pack for its multi-power hybrid powertrain. In [28], the impact of FC system and battery sizes on hydrogen consumption in a FC powered truck was examined. The study proposes the equivalent consumption minimization strategy to optimize the control setpoint for the FC and battery system utilizing a FC sub-model approach during the design phase. [5] also utilized sub-models for component modeling to propose a preliminary design methodology for a hybrid aircraft integrating FCs and batteries within the powertrain. The study presented in [29] focused on optimizing FC durability and hydrogen consumption in a FCV where the FC serves as the primary energy source, complemented by a battery. To achieve this, dynamic programming was applied to a Markov chain drive cycle model. In contrast, the work discussed in [30] specifically addresses EMS of a PFCEV. In their study, the optimization problem was expanded to include the cost associated with battery energy consumption. A global state of charge (SOC) planning method was developed based on the expected driving distance. Real-time optimization was achieved using a short-term speed predictor and a model-based rolling optimization algorithm within the predicted driving range. The research work, given in [20], employed a filtering-based power sharing strategy for a PFCEV's ESS. This approach allowed the SC to handle high dynamic power demands while utilizing the battery and the FC system for low dynamic requirements. It is worth noting that this method lacked consideration for the power consumption costs associated with each power source and did not consider PFCEV sizing aspect, resulting in a missed opportunity to achieve overall cost minimization.

In the study conducted by [22], a BEV was subjected to an optimized power allocation process through the utilization of an EMS based on model predictive control. The primary objective was to minimize energy losses and enhance the lifespan of the EV's battery. The research explored the effects of various speed predictors and time horizons on the optimization process. The results indicated that employing a Long Short-Term Memory model with a 5-second time horizon yielded the most effective approach for reducing energy losses. Furthermore, the investigation included an analysis of battery aging by employing a semi-empirical aging model, using a concept referred to as the "severity factor". In [31], the optimization of the degree of hybridization in a FC-battery EV was carried out using particle swarm optimization. The primary objective of this optimization process was to reduce the overall system cost, operational expenses, and enhance the lifespan of the battery. The study proposed two hybrid systems and determined the optimal degrees of hybridization for the hybrid powertrain under four sets of weighting factors. The simulation results provide evidence of the viability of the proposed approach. However, it is essential to acknowledge that the proposed method overlooks real-time power demands and dynamics during the optimization of degree of hybridization. It would be intriguing to explore and assess how these aspects could potentially influence factors such as battery aging or hydrogen consumption. In the study on the sizing of FC-powered ferries [3], a sensitivity analysis concerning hydrogen prices is introduced in the research. This analysis highlights that hydrogen is a main contributor in the overall expenditure and that even a slight variation in the unit price of hydrogen leads to considerable changes in the total costs involved.

1.3. Contributions

The discussion of the state-of-the-art above highlights that there has been insufficient research conducted on the CO2 emissions of EVs. This underscores the necessity for comprehensive investigations in order to acquire a profound understanding of their environmental impact. Research should consider all aspects of an EV's life cycle, including emissions associated with component production, transportation, electricity generation, and usage. While FCs are often promoted as having zero emissions, it is necessary to consider the method of hydrogen production. Despite this claim, 95% of the hydrogen used in FCs is obtained through steam methane reforming, which releases a significant amount of CO2 [32]. Green hydrogen production using renewable energy and electrolysis shows promise as a low emission-alternative. However, it is important to note that this method is more expensive compared to conventional hydrogen production methods [33]. Further research is needed to thoroughly investigate the effects of each hydrogen type on the total cost and emissions.

The aim of this study is to propose a new optimal ESS sizing for an autonomous PFCEV considering technical, economic, and environmental challenges. The vehicle power supply system consists of Li-ion batteries, SCs, and proton-exchange membrane FCs. By integrating these technologies, the PFCEV has the potential to provide a highly efficient and environmentally friendly transportation solution. According to the Ragone diagram [34], this combination effectively tackles the limitations associated with each individual technology. The study also focuses on comparing the PFCEV with other EV architectures, such as BEVs and FCVs, to determine whether the PFCEV presents any advantages over simpler vehicle designs. To achieve the required balance of performance, efficiency and cost, the ideal sizing of each component must be determined while considering their life cycle costs (LCC) and life cycle emissions (LCE). This research paper proposes a double-loop optimization approach for ESS sizing, as it is capable of simultaneously minimizing objectives during both the investment period and the operational period. It utilizes a genetic algorithm (GA) in the outer loop to identify optimal solutions with the lowest emissions, cost, and longest durability. Additionally, quadratic programming (QP) is employed in the inner loop to optimize power distribution between sources, aiming to reduce component aging and reduce driving costs. Although the concept of a double loop has been previously explored in ESS sizing studies using various algorithms [8,35,36], the unique contribution of this paper lies in the utilization of QP within the EMS. This approach actively minimizes the aging factor and driving costs, instead of solely determining an ESS size based on minimized objectives. While the temperature effect is indirectly addressed through battery current control, direct thermal management of the ESS during parking and driving phases is not included in the current study's scope.

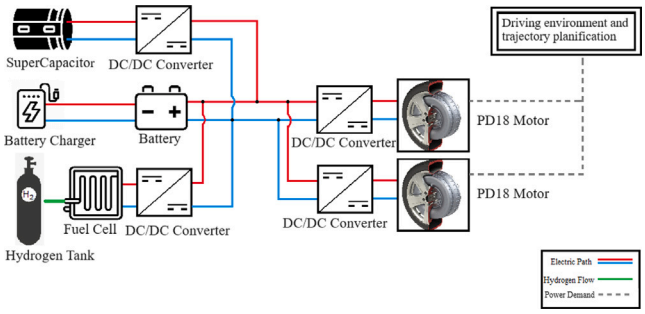

Fig. 1. Powertrain architecture.

The other contributions of this paper are as follows:

- The optimal sizing of a PFCEV that utilizes three energy sources, a battery, a FC system, and a SC while taking into consideration system cost, operation cost, battery and FC aging, and total emissions.
- The comparison of PFCEV with various EV architectures, such as BEV and FCV, serves to emphasize their individual strengths and weaknesses.
- The use of a multi-objective GA allows for many optimal solutions and display them on a three-dimensional Pareto front, considering system cost, battery aging ratio, and CO2 emissions as variables. The method is validated under different driving cycles.
- A sensitivity analysis is performed to evaluate the effects of different types of hydrogen on the sizing results.

This paper is structured as follows: Section 2 presents the EV component modeling. Section 3 develops the technique. Results from simulations are reported in Section 4. The conclusion is presented in Section 5.

2. Electric vehicle modeling

2.1. Power system topology and configuration

The powertrain configuration demonstrated in Fig. 1 presents a sustainable and effective approach for propelling EVs, utilizing renewable and clean energy sources in a semi-active topology. For more details regarding potential powertrains design and control, readers could refer to [25]. The multi-power hybrid system considered in this study integrates a FC system and a battery as the main energy sources. The FC transforms stored hydrogen into electricity, resulting in water as the sole byproduct. The system also incorporates a SC that is capable of rapidly discharging energy, making it ideal for delivering power bursts during acceleration or capturing regenerative braking energy.

The FC is connected to a unidirectional DC/DC converter, ensuring that current only flows outward from the FC and prevents any reverse current. Additionally, the SC is connected to a bidirectional DC/DC converter, enabling the voltage to be adjusted within a wide range. This flexibility enhances the efficient utilization of stored energy and power. Moreover, the battery is directly linked to the DC bus, enabling it to instantly provide any required power to the motors. In this system

architecture, the power flow from the battery is indirectly regulated by controlling the DC/DC converters connected to the FC and SC. The battery is rechargeable via an external charger, which can be connected to either a power outlet or a dedicated charging station. Alternatively, the FC can indirectly recharge the battery by generating excess energy.

Vehicle dynamics and its electromechanical drive collectively form what is referred to as the driving environment. This driving environment is susceptible to external disturbances arising from driving conditions and changes in the vehicle's speed. It interacts with the power supply system by draining power from its DC-link. The motor drive incorporates 2 in-wheel PD18 DC motors [37] connected to DC/DC converters that serve dual purposes. Firstly, during propulsion mode, they deliver the driving torque necessary for the vehicle's movement. Secondly, during braking mode, these motors act as generators, harnessing regenerative braking to charge both the SC and the battery. Fig. 2 displays the motor efficiency map and torque limits during motoring and during braking, offering a visual representation of their performance characteristics [38]. The efficiency map improves the accuracy of determining the required output power for the ESS. Once the powertrain configuration has been determined, the remaining challenges are component sizing and developing an efficient EMS to satisfy the desired objectives without diminishing vehicle performance.

2.2. Battery model

The EV's EMS utilizes the battery model to optimize the energy flow between the different sources based on driving circumstances and power requirements. By comprehending the battery's behavior, the EMS can avoid situations of overcharging or overdischarging the battery, which could have detrimental effects on the battery's chemistry and shorten its lifespan.

2.2.1. State of charge (SoC)

Eq. (1) takes into account the previous SoC at time t_{k-1}, as well as the charging and discharging powers and efficiencies, to determine the battery's SoC at a given sample time t_k [35]:

$$SoC_k = SoC_{k-1} - \int_{t_{k-1}}^{t_k} \left(\frac{P_{Bdis}}{E_B \cdot \eta_B} + \frac{\eta_B \cdot P_{Bcha}}{E_B} \right) dt \tag{1}$$

with $SoC_0 = SoC_{init}$

$$E_B = 3600 V_B \cdot Q_B, \tag{2}$$

where P_{Bdis} represents the positive discharging power of the battery at time t_k, measured in W. Secondly, P_{Bcha} refers to the negative charging power of the battery at the same time t_k, also measured in W. The efficiency of the battery's charging and discharging processes is denoted by η_B. The battery's energy capacity is represented by E_B, measured in joules. Additionally, the battery has a rated voltage V_B, measured in V, and a rated capacity Q_B, measured in Ah.

2.2.2. Battery - mass, power, LCC, and LCE

When determining the appropriate size for an ESS in an EV, it is essential to take into account the battery's mass. The battery pack constitutes one of the most substantial components in an EV, and its weight significantly influences the vehicle's overall performance, including acceleration, range, and energy consumption. It is also important to consider how the choice of battery size affects other battery characteristics. The following equations are used to derive essential battery specifications:

$$M_B = \frac{1}{3600} \cdot \frac{E_B}{\phi_{B_{ed}}} \tag{3}$$

$$P_{Bmax} = \phi_{B_{pd}} \cdot M_B \tag{4}$$

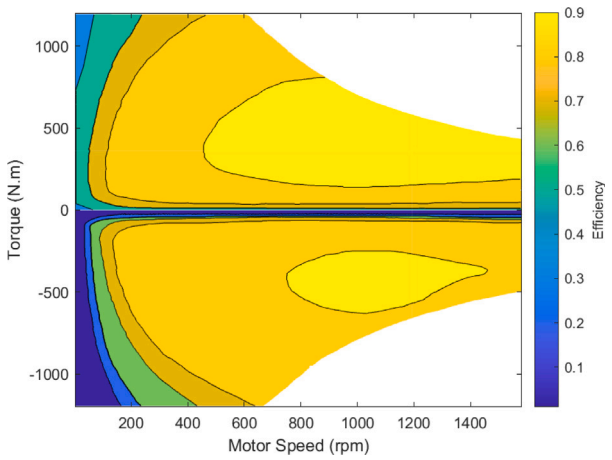

Fig. 2. Motor efficiency and torque bounds; Positive torque during motoring, negative torque during braking.

$$LCC_B = \frac{1}{3600} \cdot \phi_{B_{cost}} \cdot E_B \tag{5}$$

$$LCE_B = \frac{1}{3600} \cdot \phi_{B_{LCE}} \cdot E_B, \tag{6}$$

where the mass of the battery is represented by M_B and is measured in kg. The energy density of the battery is denoted by $\phi_{B_{ed}}$. The power density of the battery is indicated by $\phi_{B_{pd}}$. The maximal output power of the battery is denoted by P_{Bmax} and is measured in W. The LCC of the battery is represented by LCC_B and is expressed in €. The LCC per Wh of battery energy is denoted as $\phi_{B_{cost}}$. The LCE of the battery are represented by LCE_B and are measured in kg. The LCE per Wh of battery energy is indicated by $\phi_{B_{LCE}}$.

2.2.3. Aging model

In the process of designing and operating an EV's EMS, it is essential to consider battery aging as a critical factor. Over time, the battery undergoes degradation, leading to a reduction in both capacity and overall functionality. Numerous factors contribute to this aging process, such as elevated temperatures, charging and discharging cycles, depth of discharge, and operational conditions. Various methods have been utilized in prior literature to estimate battery aging, including the State of Health model [8], the Arrhenius model [31], and rainflow counting [39]. To assess the effect of battery cycles on aging, the concept of a "severity factor" is employed [40]. This factor serves as a measurement of the relative impact of each cycle on the battery's degradation compared to standard operating conditions. By incorporating the severity factor, we gain insights into the degree to which each cycle deviates from typical conditions and its contribution to the aging process of the battery. This method's advantage is that by minimizing the severity factor, it eliminates temperature increases caused by elevated current, thereby reducing accelerated aging. After neglecting the effect of battery temperature and SoC on the aging rate, the battery aging cost, $Cost_{B-Age}$, can be calculated in the following equations:

$$\sigma_k = \frac{|I_{B,k}|}{I_{nom}} \tag{7}$$

$$Ah_{eff} = \frac{1}{3600} \int_0^{t_{end}} \sigma_k \cdot |I_{B,k}| dt \tag{8}$$

$$Cost_{B-Age} = LCC_B \cdot \frac{Ah_{eff}}{Q_B \cdot N_{Cycles}}, \tag{9}$$

where the severity factor at each instant is denoted by σ_k. The charging or discharging current of the battery is represented by $|I_B|$ and is measured in A. The nominal current of the battery is indicated by I_{nom}.

The total ampere-hour Ah throughput during the drive cycle is denoted as Ah_{eff}. The number of cycles that occur during the lifetime of the battery is represented by N_{Cycles}. Finally, t_{end} represents the end time of the drive cycle.

2.3. FC model

In a PFCEV, effective power demand management and distribution are crucial for the EMS. This is primarily due to the comparatively costly consumption of hydrogen and the potential rapid depletion of the battery when subjected to high power demands.

2.3.1. Hydrogen consumption

A comprehensive onboard FC system includes various components, including the FC stack, hydrogen storage system, hydrogen circuit, air circuit, water circuit, and coolant circuit. While models for these systems tend to be complicated, this study primarily utilizes the power distribution between sources and overall efficiency to size the ESS, rather than delving into the detailed conversion processes of FCs. Previous studies have utilized the polarization curve formula to model FCs [21,30,41], while other papers have employed simplified suboptimal approaches for the FC system modeling to mitigate complexity, as is the approach taken in this study [27–29,31]. The total hydrogen consumption, M_{H_2}, is calculated using the following equation [28]:

$$M_{H_2} = \int_0^{t_{end}} \frac{P_{FC} + P_{loss}}{3.6 \cdot 10^6 \cdot LHV} dt, \tag{10}$$

where P_{FC} represents the electric power output of the FC system measured W, P_{loss} corresponds to the heat power generated by the FC system in addition to the power required for the FC auxiliary and thermal management [42], both measured in W, and LHV denotes the lower heating value of hydrogen. The efficiency of the FC system, η_{FC}, is expressed in the following equation:

$$\eta_{FC} = \frac{P_{FC}}{P_{FC} + P_{loss}} \tag{11}$$

Eq. (11) is employed to represent a quadratic model for P_{loss}, demonstrating its connection with P_{FC}. This relationship is expressed in the following equation.

$$P_{loss} = P_{FCmax} \left[a_1 \left(\frac{P_{FC}}{P_{FCmax}} \right)^2 + a_2 \frac{P_{FC}}{P_{FCmax}} + a_3 \right], \tag{12}$$

where P_{FCmax} represents the maximum power output of the FC system measured in W, and a_1, a_2, and a_3 denote coefficients determined through the process of finding the best fit for η_{FC}. In Fig. 3, the efficiency of a FC system is displayed in a normalized form. Additionally, the figure shows the best fit achieved using the model with a_1, a_2, and a_3 set to the respective values of 1.332, 0.169, and 0.172.

2.3.2. FC - mass, LCC, and LCE

Similarly to the battery, the following equations are used to derive essential FC specifications:

$$M_{FC} = \frac{P_{FCmax}}{\phi_{FCpd}} \tag{13}$$

$$LCC_{FC} = \phi_{FC_{cost}} \cdot P_{FCmax} \tag{14}$$

$$LCE_{FC} = \phi_{FC_{LCE}} \cdot P_{FCmax} \tag{15}$$

$$M_{Tank} = \phi_{Tank_d} \cdot M_{H_2max} \tag{16}$$

$$E_{FC} = 3.6 \cdot 10^6 \cdot M_{H_2max} \cdot LHV \cdot \eta_{FC} \tag{17}$$

$$LCC_{Tank} = \phi_{Tank_{cost}} \cdot E_{FC}, \tag{18}$$

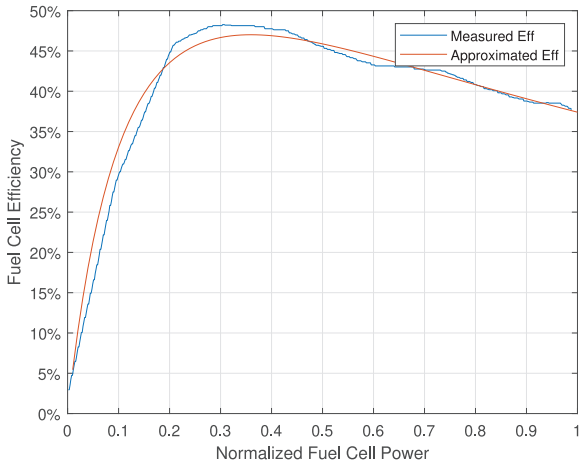

Fig. 3. Normalized efficiency of a FC system [31] and Best Fit Model.

where the mass of the FC system (excluding the hydrogen tank), denoted as M_{FC}, is measured in kg. The power density of the FC system, represented by ϕ_{FCpd}. The LCC of the FC system, denoted as LCC_{FC}, is measured in €. The LCC per W of FC rated power, represented as $\phi_{FC_{cost}}$. The LCE of the FC syste, denoted as LCE_{FC}, is measured in kg. The LCE per W of FC rated power, represented by $\phi_{FC_{LCE}}$. Additionally, the system includes a hydrogen tank with a mass of M_{Tank}, measured in kg. The mass of the tank per kg of stored hydrogen, denoted as ϕ_{Tank_d}, M_{H_2max} represents the maximum mass of hydrogen that can be stored, measured in kg, and E_{FC} is the net output energy of the FC system, measured in joules. The LCC of the hydrogen tank, represented by LCC_{Tank}, is measured in €. Finally, the LCC per kWh of stored hydrogen, denoted as $\phi_{Tank_{cost}}$.

2.3.3. FC aging

Multiple research studies [29,30,43,44] have highlighted that the lifespan of FCs utilized in automobiles tends to be shorter compared to stationary FCs. This discrepancy can be primarily attributed to the specific operating conditions encountered by automotive FCs. The typical driving cycle comprises rapid load fluctuations (exceeding a change of 10% of rated power per second), frequent starts and stops in urban traffic, idling during halts (with the FC operating at less than 5% of its rated power), and periods of high power demand (with the FC operating at over 95% of its rated power). All these factors collectively contribute to the degradation and reduced longevity of FCs in automotive applications as shown in the following equation:

$$T_f = \frac{\Delta P}{k_p(P_1 n_1 + P_2 n_2 + P_3 t_1 + P_4 t_2)}, \tag{19}$$

where ΔP represents the maximum allowable value for FC voltage degradation in a vehicle equal to 10%. Notably, P_1, P_2, P_3, and P_4 denote the performance degradation rates associated with load changes, start-stop events, idling, and heavy load conditions, respectively. Moreover, n_1, n_2, t_1, and t_2 represent the corresponding quantities, such as the number of load change cycles, start-stop cycles, idling time, and heavy load time present in the driving cycle. To account for variations in FCs, the correction factor k_p is introduced.

In this paper, these conditions will be later prevented using constraints to decrease the computation complexity (refer to Section 3.2).

2.4. SC model

In EVs, SCs are frequently employed to provide additional power during periods of high demand, such as acceleration and regenerative braking. SCs are often regarded as a beneficial supplement to batteries due to their high power density. By assisting in reducing the load on batteries, SCs can effectively prolong their lifespan.

2.4.1. State of voltage (SoV)

The following equation takes into account the previous SoV at time t_{k-1} as well as the power and efficiency to find the SoV at time t_k:

$$SoV_k = SoV_{k-1} - \int_{t_{k-1}}^{t_k} \left(\frac{P_{SCdis}}{\eta_{SC} \cdot E_{SC}} + \frac{\eta_{SC} \cdot P_{SCcha}}{E_{SC}} \right) dt \tag{20}$$

With $SoV_0 = SoV_{init}$

$$E_{SC} = 0.5 Q_{SC} \cdot V_{SC}^2, \tag{21}$$

where P_{SCdis} represents the positive discharge power of the SC at time t_k, measured in W. Similarly, P_{SCcha} denotes the negative charge power of the SC at time t_k, also measured in W. η_{SC} represents the charging and discharging efficiency of the SC. E_{SC} represents the energy capacity of the SC, measured in joules. V_{SC} corresponds to the rated voltage of the SC. Lastly, Q_{SC} denotes the rated capacity of the SC, measured in farads.

2.4.2. SC - mass, power, LCC, and LCE

Similarly to the other sources, the critical specifications will calculated using the following equations:

$$M_{SC} = \frac{1}{3600} \cdot \frac{E_{SC}}{\phi_{SC_{ed}}} \tag{22}$$

$$P_{SCmax} = \phi_{SC_{pd}} \cdot M_{SC} \tag{23}$$

$$LCC_{SC} = \frac{1}{3600} \cdot \phi_{SC_{cost}} \cdot E_{SC} \tag{24}$$

$$LCE_{SC} = \frac{1}{3600} \cdot \phi_{SC_{LCE}} \cdot E_{SC}, \tag{25}$$

where M_{SC} represents the mass of the SC, measured in kg. $\phi_{SC_{ed}}$ denotes the energy density of the SC. $\phi_{SC_{pd}}$ signifies the power density of the SC. P_{SCmax} represents the maximal output power of the SC, measured in W. Additionally, LCC_{SC} denotes the LCC of the SC, measured in €, while $\phi_{SC_{cost}}$ represents the LCC per Wh of SC energy. Moreover, LCE_{SC} signifies the LCE of the SC, measured in kg, and $\phi_{SC_{LCE}}$ represents the LCE per Wh of SC energy.

2.4.3. SC aging

Numerous studies have explored the aging phenomenon of SCs by employing various models. For example, in [34], a cycle counting model was utilized to assess and quantify SC aging. Additionally, [45] investigated SC aging and estimated its lifespan by applying the Arrhenius law. However, in the current study, SC aging will not be considered due to the extensive cycle count and relatively low cost of SCs compared to other primary energy sources, as it serves as a secondary energy source.

2.5. Vehicle model

The vehicle dynamic equation has been a key component in numerous prior studies, including those referenced as [8,27,30]. In this particular study, the focus revolves around estimating several factors. These include determining the power requirements for a specific driving cycle, calculating the maximum achievable speed of the vehicle, assessing the acceleration time required to reach a certain speed, determining the maximum climbing angle the vehicle can handle, and estimating the overall driving mileage achievable by the vehicle.

2.5.1. Dynamic equation

The equation provided is utilized to determine the amount of power required by the vehicle to follow the driving cycle depicted in Fig. 4.

$$P_m \eta_T \eta_{md} = mgF_r u \cos(\theta) + 0.5 \rho C_d A u^3 + mg \sin(\theta) u + mu \frac{du}{dt} \tag{26}$$

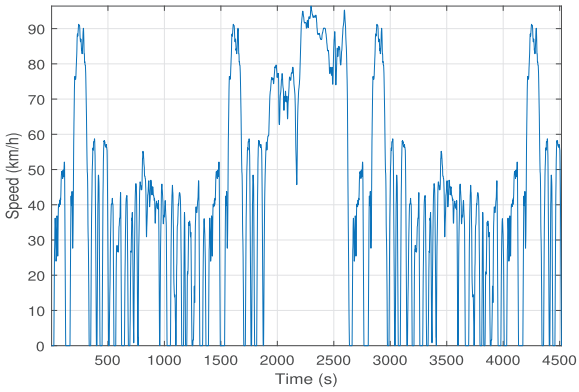

Fig. 4. UDDS drive cycle.

where P_m represents the power required for the vehicle, measured in W. The transmission efficiency is denoted by η_T. The motor drive efficiency is represented by η_{md} and has a variable value indicated in Fig. 2. The density of air is denoted by ρ. The drag coefficient of the vehicle is represented by C_d. The frontal area of the vehicle is denoted by A. The velocity of the vehicle is represented by u and is measured in m/s. The mass of the vehicle including the ESS is denoted by m. The acceleration due to gravity is represented by g. The coefficient of rolling resistance is denoted by F_r. Lastly, the angle of the slope is represented by θ and is measured in radians.

The chosen driving cycle has been designed to closely mimic the typical daily driving cycles of humans. It incorporates the "in-city" segment of the Urban Dynamometer Driving Schedule (UDDS), which involves frequent instances of starting and stopping, as well as a series of rapid acceleration and deceleration events. Following this, a "highway" section of the UDDS is included, where higher speeds are reached to account for fuel consumption and heavy load conditions. The sequence then returns to the initial part of the cycle to complete the pattern. It is important to note that the entire cycle assumes a flat asphalt terrain ($\theta = 0$, $F_r = 0.02$ [46]). However, in this project, it is essential to emphasize that the considered autonomous vehicle possesses prior knowledge of the speed profile, enabling it to navigate the driving cycle optimally. Furthermore, it is also important to mention that in this study, the specified power is exclusively allocated for propelling the vehicle and does not include the power needs of auxiliary and cooling systems, as these aspects are beyond the scope of our work.

2.5.2. Maximum speed

The needed power to reach a certain maximum speed u_{max} can be obtained from Eq. (26) when $\frac{du}{dt} = 0$ and $\theta = 0$ [27].

$$P_{Bmax} + P_{FCmax} + P_{SCmax} \geq \frac{mgF_r u_{max} + 0.5 \rho C_d A u_{max}^3}{\eta_T \eta_{md}} \tag{27}$$

In this formula, a constant value of 0.8 is assumed for η_{md} to quantify this particular value.

2.5.3. Acceleration time

The accelerating time is commonly employed as a metric to assess a vehicle's acceleration capability. It is defined as the duration it takes for a vehicle to accelerate from a standstill to a specific speed, denoted as u_1. Similar to determining the maximum speed, this evaluation is

conducted on flat surfaces. During the acceleration phase, the discrete velocity is calculated using the following method [27].

$$\begin{cases} u(0) = 0 \\ u(k) = \dfrac{F(k)\Delta t}{m} + u(k-1) \\ F(k) = \dfrac{\tau_m(k)\eta_T}{r} - mgF_r - 0.5\rho C_d A u(k-1)^2 \\ \tau_m = min\left(\tau_{allowed}(k), \eta_{md}\dfrac{P_{Bmax} + P_{FCmax} + P_{SCmax}}{\omega(k)}\right) \end{cases} \tag{28}$$

where F represents the drive force, Δt denotes the sample time, and k signifies the discrete time index. τ_m corresponds to the maximum torque of the electric motor, which is determined by the torque bounds of the motor shown in Fig. 2, and the output capabilities of the sources. ω represents the rotational speed of the electric motor. Additionally, the maximum value on the torque bounds curve at $\omega(k)$ corresponds to the allowable maximum torque of the electric motor, denoted as $\tau_{allowed}$, and r represents the tire radius. The accelerating time, t_a, refers to the duration from the beginning to the end of the acceleration period and is calculated as follows:

$$t_a = N\Delta t, \tag{29}$$

where N represents the index of the discrete time instance when the vehicle reaches the target velocity u_1

2.5.4. Maximum climbing angle

By considering the very small climbing velocity when a vehicle reaches its maximum climbing angle θ_{max}, the rate of change of velocity $\frac{du}{dt}$ is equal to zero and u^3 approaches zero, the following equation is obtained [27]:

$$F_r \cos\theta_{max} + \sin\theta_{max} = \frac{\tau_m \eta_T}{mgr} \tag{30}$$

2.5.5. Maximum range

Typical range measurements for commercial vehicles often adhere to established drive cycles such as the UDDS, Worldwide Harmonized Light Vehicles Test Procedure (WLTP), or New European Driving Cycle (NEDC) when conducted on a dynamometer [47]. As done in previous similar literature [8,27,48], this study employs a simplified approach, where a flat road and a constant speed u_0 (set at 60 km/h) are assumed to estimate the necessary energy in the ESS to meet a specific range requirement.

$$L = \frac{(SoC_{max} - SoC_{min})E_B + E_{FC} + E_{SC}}{mgF + 0.5\rho C_d A u_0^2}, \tag{31}$$

where SoC_{min} (20%) and SoC_{max} (80%) are the lower and upper values for the SoC.

3. Methodology

In this study, a combined multi-objective optimization approach was employed to develop a sizing and EMS model. The approach comprises two interconnected loops: an outer loop implemented using a genetic algorithm (GA) and an inner loop solved using quadratic programming (QP). The GA-driven outer loop aims to derive the ideal sizing vector for the ESS, taking into account variables like Battery Capacity, FC system Power, SC Capacity, and Hydrogen Limit. Notably, this process involves simultaneously adjusting and optimizing these parameters, in contrast to approaches that focus on altering one parameter while holding others constant as in [9]. This simultaneous adjustment enables a more comprehensive exploration of the solution space, potentially leading to more effective ESS configurations. The objective of the optimization is to minimize the following values:

- CO2 emissions per km.
- System and operation costs.

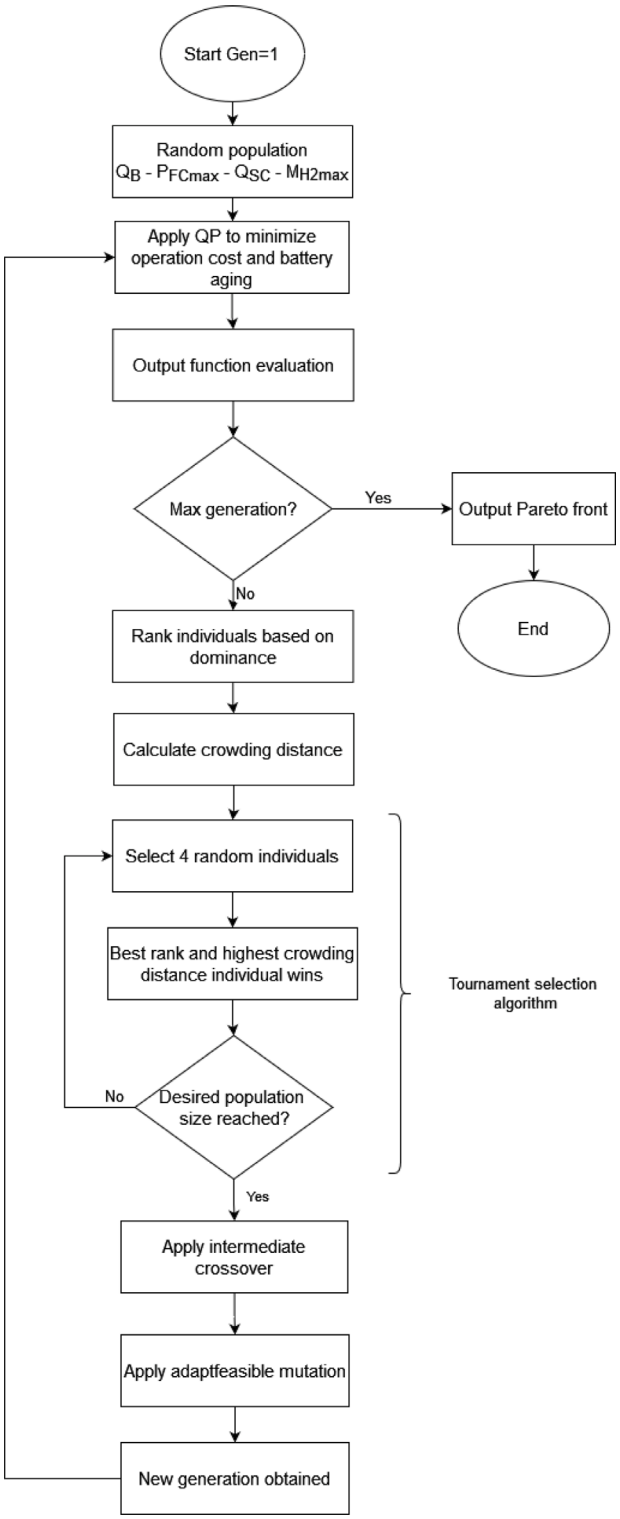

Fig. 5. Optimization flow chart.

- Relative battery degradation.

The optimization model utilized in this study incorporates an inner loop consisting of a QP algorithm and an economic function. The sizing vector, obtained from the GA algorithm, is fed into the QP algorithm, which determines the optimal power flow allocation with the aim of minimizing operation costs and battery degradation, as depicted in Fig. 5, while FC durability is considered in the constraints. The

ultimate objective of the optimization model is to achieve a Pareto Front, which graphically represents the optimal sizing solutions within a given budget constraint while simultaneously minimizing both CO2 emissions and battery degradation.

3.1. Inner loop - quadratic programming

3.1.1. Cost function

As previously stated the objective of QP is to minimize both the operations cost and the battery aging cost throughout the drive cycle using the following cost function:

$$CF = \int_0^{t_{end}} \frac{\sigma_{ChaP}}{3.6 \cdot 10^6} \cdot \left(\frac{P_{Bdis}}{\eta_{Bdis}} + \eta_{Bcha} \cdot P_{Bcha} \right) dt + \int_0^{t_{end}} \frac{\sigma_{H_2P}}{3.6 \cdot 10^6 \cdot LHV} \cdot \left(P_{FC} + P_{loss} \right) dt + Cost_{B-Age} \tag{32}$$

the cost function in this context comprises three components. The first component is associated with the cost of electrical energy supplied by the battery, which must be replenished subsequently, with σ_{ChaP} representing the cost per kWh of electricity. The second component represents the cost of hydrogen consumption, with σ_{H_2P} representing the cost per kg of hydrogen. The third and final component accounts for the economic impact of battery aging and is expressed through Eqs. (7) to (9).

3.1.2. Constraints

Constraints are incorporated in the system to maintain the battery and FC within safe operating limits, preventing hazardous conditions that could potentially damage the components or reduce their lifespan. Deep discharges and overcharges are known to have detrimental effects on battery longevity. By restricting the SoC of the battery within a certain range, it is possible to extend its lifespan, as indicated by the following constraint [40].

$$SoC_{min} \leq SoC \leq SoC_{max} \tag{33}$$

To ensure that the components operate within safe limits and maintain a proper power balance between the source and load, the constraints listed below are employed:

$$0 \leq P_{Bdis} \leq P_{Bmax} \tag{34}$$

$$-P_{Bmax} \leq P_{Bcha} \leq 0 \tag{35}$$

$$0 \leq P_{SCdis} \leq P_{SCmax} \tag{36}$$

$$-P_{SCmax} \leq P_{SCcha} \leq 0 \tag{37}$$

$$0.05 P_{FCmax} \leq P_{FC} \leq 0.95 P_{FCmax} \tag{38}$$

$$-0.1 P_{FCmax} \leq \Delta P_{FC} \leq 0.1 P_{FCmax} \tag{39}$$

$$P_{Bdis} + P_{Bcha} + P_{SCdis} + P_{SCcha} + P_{FC} = P_m \tag{40}$$

$$SoV_{t_{end}} \geq SoV_{init} \tag{41}$$

$$P_{Bdis} \cdot \left(P_m - 0.05 P_{FCmax} \right) \geq 0 \tag{42}$$

$$P_{Bcha} \cdot \left(P_m - 0.05 P_{FCmax} \right) \geq 0 \tag{43}$$

$$P_{SCdis} \cdot \left(P_m - 0.05 P_{FCmax} \right) \geq 0 \tag{44}$$

$$P_{SCcha} \cdot \left(P_m - 0.05 P_{FCmax} \right) \geq 0 \tag{45}$$

To ensure the protection of the FC against unfavorable conditions such as high power demands, frequent start-stop operations, unnecessary idling, and rapid load changes, constraints (38) and (39) are applied. These constraints are discussed in detail in Section 2.3.3, as they are necessary for preserving the FC's lifespan. By implementing this approach, the FC system is only switched off when the vehicle is turned off. Constraints (42) to (45) mandate the battery and SC to discharge only when power is required and charge only when there is excess power. This prevents the algorithm from recommending simultaneous charging and discharging of the sources. Additionally, to consider both the battery and the FC in the optimization of sizing, it is recommended to set the initial SoC to 45%. This approach is well-suited for architectures that rely on the battery for short distances and the FC for extended range. By doing so, EMS can effectively consider both components, preventing it from prioritizing the battery and neglecting the FC.

3.2. Outer loop - genetic algorithm

3.2.1. Cost function

The multi-objective GA uses the power allocation from QP to determine the value of each objective. The first objective, Obj_1, is to calculate the total economic cost of the vehicle, which includes investment and operational costs (also known as CapEx and OpEx). The second objective, Obj_2, is to evaluate the battery aging factor, while the third objective, Obj_3, is to assess the total CO2 emissions of the vehicle, taking into account its LCE and operational emissions. These calculations are performed with the assumption that the vehicle will be driven daily for a period of ten years (3650 days), which corresponds to a distance of 190,000 km based on the used drive cycle.

$$Obj_1 = 3650 \int_0^{t_{end}} \frac{\sigma_{ChaP}}{3.6 \cdot 10^6} \cdot \left(\frac{P_{Bdis}}{\eta_{Bdis}} + \eta_{Bcha} \cdot P_{Bcha} \right) dt + 3650 \int_0^{t_{end}} \frac{\sigma_{H_2P} \cdot \left(P_{FC} + P_{loss} \right)}{3.6 \cdot 10^6 \cdot LHV \cdot \eta_{FC}} dt + LCC \tag{46}$$

With $LCC = LCC_B + LCC_{FC} + LCC_{Tank} + LCC_{SC}$

$$Obj_2 = 3650 \frac{Cost_{B-Age}}{LCC_B} \tag{47}$$

$$Obj_3 = 3650 \int_0^{t_{end}} \frac{\sigma_{ChaE}}{3.6 \cdot 10^6} \cdot \left(\frac{P_{Bdis}}{\eta_{Bdis}} + \eta_{Bcha} \cdot P_{Bcha} \right) dt + 3650 \int_0^{t_{end}} \frac{\sigma_{H_2E} \cdot \left(P_{FC} + P_{loss} \right)}{3.6 \cdot 10^6 \cdot LHV \cdot \eta_{FC}} dt + LCE \tag{48}$$

With $LCE = LCE_B + LCE_{FC} + LCE_{SC}$

With σ_{ChaE} being the carbon emissions per kWh of electricity and σ_{H_2E} being the carbon emissions for producing 1 kg of hydrogen through steam methane reforming which is the primary method for hydrogen production.

3.2.2. Constraints

When searching for the optimal sizing of an ESS, it is important to ensure that driving performance requirements such as maximum speed u_{max}, acceleration time t_a, maximum climbing angle θ_{max} and mileage L are guaranteed using Eqs. (27), (29), (30), and (31), as well as the following constraints:

$$u_{max} \geq 150 \text{ km/h} \tag{49}$$

$$t_a \leq 14 \text{ s} \tag{50}$$

$$\theta_{max} \geq 15 \text{ deg} \tag{51}$$

$$L \geq 600 \text{ km}. \tag{52}$$

By constraining the search space, the genetic algorithm can concentrate on a particular region where reasonable, feasible and optimal solutions are anticipated, facilitating a quicker and more efficient search process. The decision variables are bounded by the following constraints:

$$10 \text{ Ah} \leq Q_B \leq 100 \text{ Ah} \tag{53}$$

$$1 \text{ kW} \leq P_{FCmax} \leq 50 \text{ kW} \tag{54}$$

$$1 \text{ Farads} \leq Q_{SC} \leq 50 \text{ Farads} \tag{55}$$

$$3 \text{ kg} \leq M_{H_2max} \leq 10 \text{ kg} \tag{56}$$

4. Simulation results

The integrated multi-objective optimization method outlined in Section 3 is utilized to determine the most optimal sizing for the ESS of a PFCEV. The simulation has been conducted using MATLAB with a time step of $T_s = 1$ s. The choice of the *quadprog* function for QP is due to the quadratic nature of the cost function resulting from the battery aging model and the FC model. Additionally, the *gamultiobj* function has been employed for the GA aspect of the simulation, involving the algorithms for selection, crossover, and mutation phases of GA [49]. The generation count was configured to 100, each consisting of a population size of 70, and a crossover fraction of 0.8. All other relevant technical and economic parameters that have been taken into account can be found in Tables 1 and 2. Subsequently, the obtained results of the optimization process for sizing are presented. To illustrate the optimal power distribution between the sources, a specific solution is selected as an example. In order to asses the robustness of the methodology, the objectives will be computed by applying different driving conditions to the optimal sizing result obtained. Lastly, a comparative analysis is conducted among various types of EVs, followed by a sensitivity analysis concerning the type of hydrogen utilized. This is done to showcase their influences on the sizing results.

Table 1
Technical parameters.

	Variable	Value
Battery	η_B	0.97 [28,35,50]
	V_B	400 V
	$\phi_{B_{ed}}$	150 Wh/kg [51]
	$\phi_{B_{pd}}$	1000 W/kg
	I_{nom}	1 C-rate
	N_{Cycles}	3000 Cycles [40]
	SoC_{init}	0.45
	SoC_{min}	0.2
	SoC_{max}	0.8
FC	η_{FC}	0.4
	ϕ_{FCpd}	1600 W/kg
	ϕ_{Tank_d}	20 kg/kgH2
	LHV	33.33 kWh/kg
SC	η_{SC}	0.95
	V_{SC}	200 V
	$\phi_{SC_{ed}}$	6 Wh/kg [52]
	$\phi_{SC_{pd}}$	3500 W/kg
	SoV_{init}	0.5
Vehicle	ρ	1.29 kg/m^3
	C_d	0.335
	F_r	0.02 [46]
	A	2 m^2
	m	1480 kg
	g	9.81 m/s^2
	r	0.35 m
	η_T	0.9

Table 2
Economical parameters.

	Variable	Value
Battery	$\phi_{B_{cost}}$	158 €/kWh [53]
	$\phi_{B_{LCE}}$	80 kgCO2/kWh [54]
	σ_{ChaP}	0.2 €/kWh [55]
	σ_{ChaE}	58 gCO2/kWh [56]
FC	$\phi_{FC_{cost}}$	75 €/kW [57]
	$\phi_{FC_{LCE}}$	57 gCO2/kW [58]
	$\phi_{Tank_{cost}}$	10 €/kWh [59]
	σ_{H_2P}	3.5 €/kg
	σ_{H_2E}	8900 gCO2/kg [32]
SC	$\phi_{SC_{cost}}$	10 €/Wh [60]
	$\phi_{SC_{LCE}}$	2000 gCO2/Wh [52]

4.1. PFCEV sizing

4.1.1. UDDS drive cycle case

After applying the optimization algorithm, a set of 29 solutions is presented on a Pareto front in Fig. 6. Each data point on the graph represents the total cost in €, the battery aging factor, and the CO2 emissions per km in g associated with each solution. A particular solution has been chosen as a prime example for component behavior analysis due to its combination of low cost, minimal emissions, and an acceptable battery aging factor. This solution includes a 41 Ah battery, 5.7 kW FC power, 4 Farads SC capacity, and 7.4 kg of stored hydrogen. This well-balanced solution has a total cost of 11,917 €, which includes an investment cost of 5752 € and a driving cost of 3.24 €/100 km. Additionally, this solution emits 60 gCO2/km and has a battery aging ratio of 0.5 after 10 years of use, the ESS total weight contributes approximately 18% of the total weight of the PFCEV. To show EMS performance Fig. 7 depicts the optimal distribution of power within the ESS described previously, showcasing the successful execution of each component's designated role to satisfy the power demand. The FC delivers a consistent power flow to the motor, mitigating the risk of rapid aging by avoiding sudden power fluctuations, high power utilization, and even idling during braking phases, by applying the FC aging model specified in Eq. (19), a near zero deterioration rate is calculated. The battery manages the majority of the power requirements and shows quick responsiveness to abrupt changes in power demand. Moreover, the SC steps in to absorb instances of peak regenerative power during braking, while also providing assistance to the battery during acceleration. This collaboration effectively safeguards the battery against the impact of high currents, leading to a prolonged operational lifespan. The contribution of each component towards the overall cost and emissions during its lifetime is displayed in Figs. 8 and 9. The findings reveal that conventional hydrogen consumption, despite the FC delivering less power compared to the battery, contributes to approximately 32% of the total cost and 80% of the total emissions, larger than the 21% cost and 6% emissions stemming from electricity purchase. Furthermore, the investment cost associated with a FC system incorporating hydrogen storage is similar to a battery system capable of delivering significantly higher power output. This implies that relying on the FC to mitigate battery aging would lead to a more expensive EV to operate, coupled with higher CO2 emissions, as shown by the high cost and emission solutions on the Pareto front. These outcomes prove the importance of adopting greener techniques for hydrogen production to drive down overall emissions while keeping hydrogen prices low.

In Fig. 10(a), the sizing results for each solution on the Pareto Front are illustrated, along with the total economic cost of each solution. Hydrogen storage limit appears to be constant to fulfill the high range requirement. Furthermore, it becomes apparent that the increased costs and emissions of the ESS are linked to the inclusion of a large battery and SC, along with a powerful FC. Apart from the substantial initial

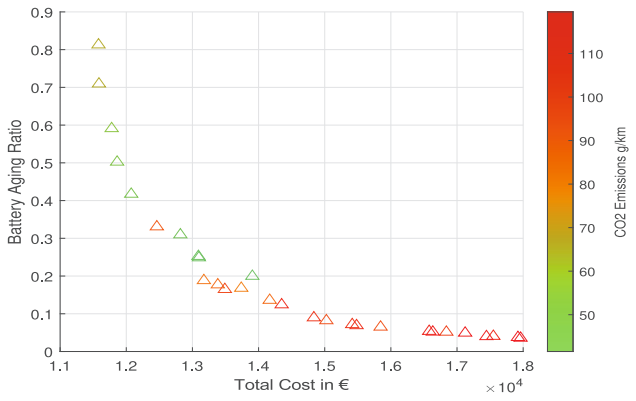

Fig. 6. Pareto Front of the sizing optimization result for the PFCEV.

investment, this is also attributed to the utilization of conventional hydrogen for electricity generation, which leads to increased costs and greater CO2 emissions compared to externally charging the battery. These solutions exhibit the least amount of degradation due to the prioritization of minimizing aging over minimizing costs, which is reflected in the design of the ESS to be larger than necessary. For solutions characterized by low cost and high battery aging, the proposed sizing tends to lean towards the lower end. This suggests that the ESS is designed to just meet performance and durability constraints while minimizing costs as much as possible, even if it means approaching the lower limit of what might be considered optimal sizing. For balanced solutions that exhibit medium cost, battery degradation and emissions (i.e. solutions ranging between 12,000 € to 14,000 € for this case study), the ESS sizing alternates between a high battery capacity paired with a low FC power, or a high FC power paired with a small battery. Fig. 10(b) displays the mass of the ESS for each sizing outcome, along with its weight relative to the total vehicle weight of 1480 kg. Upon examination of the figure, it becomes apparent that a high weight associated with the high cost and low battery aging solutions indicates that the system size relatively large. While, a low weight associated with the low cost and high battery aging solutions implies that the system is smaller than what might be considered optimal.

4.1.2. Robustness check

The previous sizing results were obtained using a UDDS drive cycle, which includes diverse driving scenarios including frequent stops and sustained high-speed driving, as illustrated in Fig. 4. To evaluate the robustness of the study, it is important to analyze the impact of varying driving conditions on these sizing results. For this reason, the WLTP drive cycle will be considered in the next.

In this section, firstly, the inner loop of the presented method is used to generate the power allocation for a WLTP drive cycle within a PFCEV using the UDDS-based ESS sizing depicted in Fig. 10(a). However, the corresponding objectives achieved (total cost, battery degradation, and total emissions) may not be optimal since the ESS was not sized specifically for the WLTP drive cycle. Secondly, in order to evaluate the robustness of UDDS-based sizing, we will calculate the optimal sizing associated with the WLTP drive cycle, and then compare these optimal objectives with those associated with the power allocation done on the UDDS-based sizing for WLTP. To ensure fairness in the comparison, the results will be conducted under the assumption of the same total driven distance of 190,000 km mentioned in Section 3.2.1.

The WLTP drive cycle, depicted in Fig. 11, is segmented into four distinct sections characterized by varying average speeds: low, medium, high, and extra high. While it features a shorter duration and distance compared to the previous drive cycle, it attains a higher top speed.

Fig. 12 illustrates the Pareto front of objectives resulting from applying a WLTP drive cycle to the previous UDDS-based sizing, alongside the Pareto front associated with an optimal sizing based on WLTP. Both fronts exhibit a similar trend in the trade-off between cost, battery aging, and CO2 emissions. The power allocation of WLTP done on UDDS-based sizing, on average, show approximately 3% higher cost, 9% more emissions, and 7% more battery aging compared to the optimal results. This slight discrepancy validates the methodology for PFCEV sizing optimization.

4.2. Comparative analysis

This part focuses on a comparative analysis involving the PFCEV alongside less complex vehicle types, such as the BEV and FCV, with the intention of showing the potential benefits attributed to a more complex design aimed at meeting the required performance standards.

In this study, the BEV's ESS depends solely on a battery as the primary energy source, excluding the FC system, with a SC serving as a secondary source to support during high power demands or when regenerative energy is utilized. This setup means their primary energy source comes from external charging. On the other hand, the FCV's ESS uses a FC system as its primary energy source, while a battery serves as a secondary energy store. This battery is designed to be rechargeable internally through regenerative braking or from the FC. Importantly, the BEV operates within the same operational conditions and constraints as the PFCEV for the used sources. However, in the FCV, adjustments are made to the battery to ensure a final SoC exceeding 50%, a measure taken to guarantee sufficient energy availability for future drives, as done for the PFCEV in constraint (41).

Fig. 13 illustrates distinct Pareto fronts corresponding to each vehicle type. The solutions associated with BEVs exhibit notably elevated costs, averaging approximately 157% higher than those of PFCEVs. This discrepancy can be attributed to the mileage constraint that necessitates a relatively large battery in BEVs, consequently leading to a lower aging rate.

Conversely, FCVs exhibit an average cost that is approximately 14% higher than that of PFCEVs, while maintaining a similar aging ratio. However, it is important to note that FCVs emit 55% more CO2 than PFCEVs. In the pursuit of ESS investment minimization and driving cost optimization and emissions reduction in the transportation sector, PFCEVs prove to be the better choice.

4.3. Sensitivity analysis

To highlight the impact of utilizing green hydrogen instead of conventional hydrogen on the results, this section centers on a sensitivity analysis employing a different value for hydrogen pricing and emissions. It is approximated that producing 1 kg of hydrogen demands around 55 kWh of electricity. The carbon footprint and price exhibit significant variability based on the energy source utilized. For the purpose of this analysis, a carbon footprint of 3 kgCO2/kgH2 [61] is assumed, and the price is fixed at 8 €/kgH2 [62].

The resulting Pareto front achieved through these modifications is showcased in Fig. 14, alongside the Pareto front representing the conventional hydrogen case as depicted in Fig. 6. On average, solutions linked to green hydrogen exhibit a cost that is approximately 12% higher than those tied to conventional hydrogen. However, these solutions emit 165% less CO2. This discrepancy can be attributed to the higher cost and reduced carbon footprint associated with green hydrogen. In Fig. 15, the sizing solutions are presented for both scenarios involving green and conventional hydrogen. For cost optimization with green hydrogen, it is beneficial to prioritize a larger battery capacity and use it as the main energy source. This strategy is more economical compared to relying on the FC system, which could lead to increased driving costs due to the higher price of hydrogen. In scenarios involving green hydrogen, the FC system functions as a range extender, providing a consistent but minimal power output while minimizing hydrogen consumption. This trend is evident in the sizing results, where the

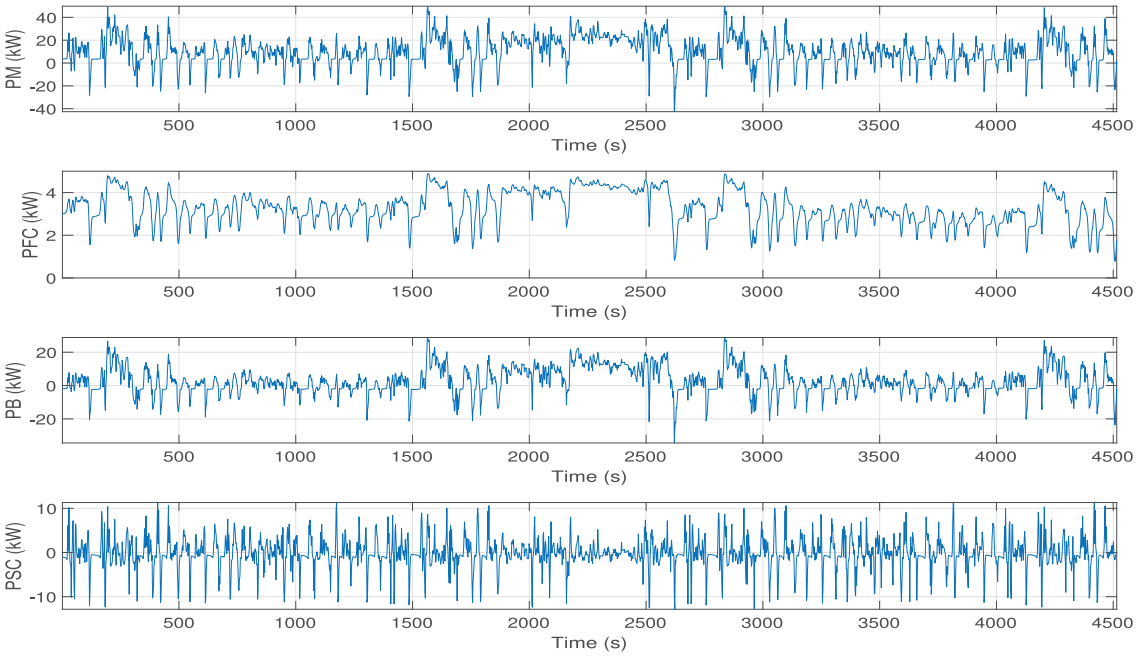

Fig. 7. Optimal power allocation.

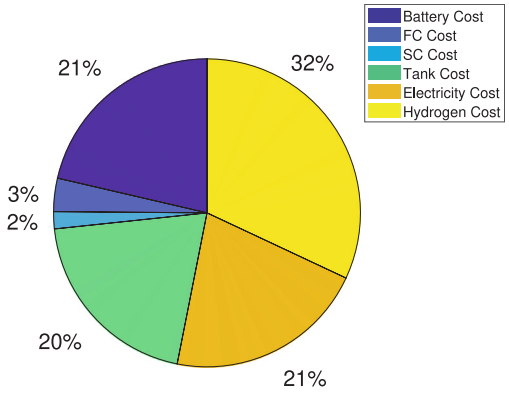

Fig. 8. Components cost contributions.

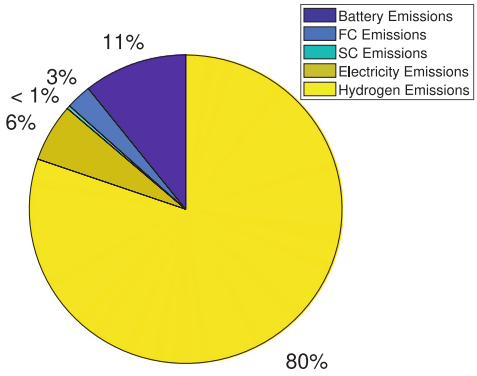

Fig. 9. Components CO2 emission contributions.

battery capacity is higher and the FC power is lower in comparison to the conventional hydrogen case. Moreover, the SC capacity and Tank storage exhibit reduced values, as the large battery capacity serves as a compensates in energy storage. In order to make this environmentally friendly option economically viable and efficient, the cost of producing green hydrogen must be lowered significantly.

5. Conclusion and perspectives

The study focuses on the optimal sizing of a PFCEV ESS, that uses a battery, a FC system and a SC. Presented as a multi-objective problem, the study places priority on minimizing FC and battery aging, CO2 emissions and costs. To examine how component sizing affects battery durability, the study integrated an aging model that incorporates a severity factor. Additionally, the study also imposed driving performance requirements as constraints for optimization.

The implementation of a QP EMS algorithm facilitated the allocation of power among various sources, aiming to minimize driving costs and battery aging, while also protecting the FC from deterioration. Moreover, a GA was employed to find a feasible solution domain that satisfies the set constraints. In summary, the results, as depicted in Figs. 6 to 10(b), provide valuable insights into optimal sizing recommendations for PFCEV ESS.

Through a comparative analysis involving PFCEVs, FCVs, and BEVs that share the same driving performance requirements, it is evident that PFCEVs emerge as the superior choice in terms of ESS total cost reduction and emissions reduction shown in Fig. 13. Additionally, a sensitivity analysis concerning hydrogen type emphasizes the need for decreased costs of green hydrogen to enhance its economic feasibility and operational efficiency. This necessity is highlighted through the results presented in Figs. 14 and 15.

In our future work, we plan to enhance, utilize, and compare alternative meta-heuristic methods to enhance the convergence of the solutions in the outer loop. It is also suggested to improve the modeling of the system by incorporating the electro-chemical FC model and the non-linear Arrhenius model to address aging effects influenced

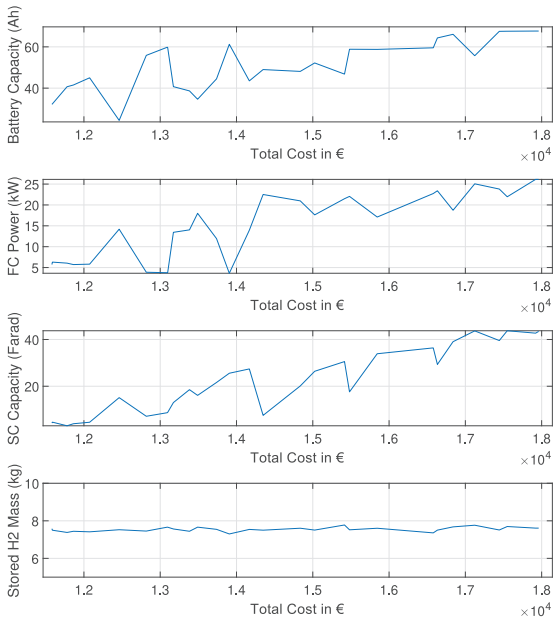

(a)

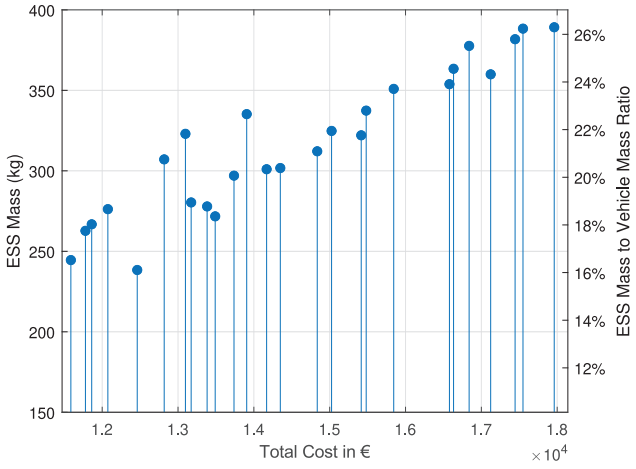

(b)

Fig. 10. (a) Sizing result for the PFCEV, (b) ESS Mass for the PFCEV.

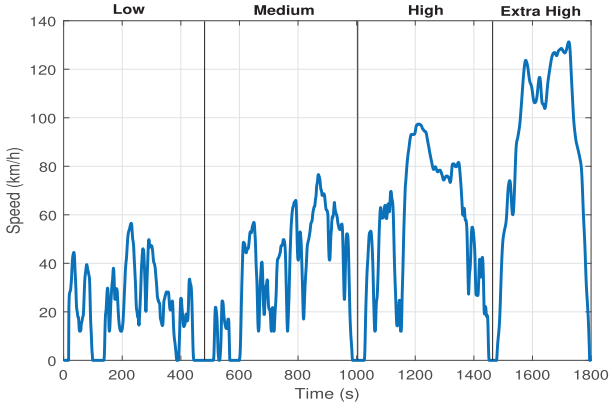

Fig. 11. WLTP drive cycle.

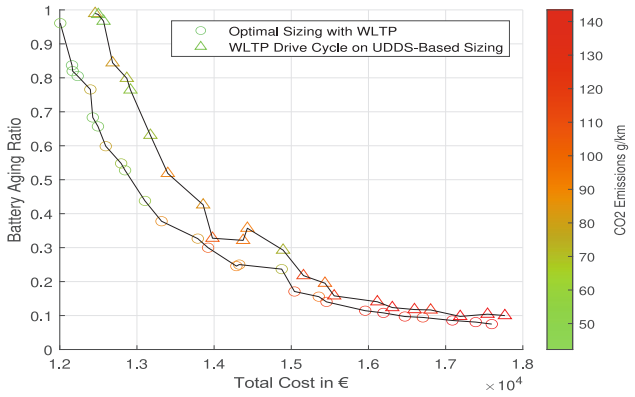

Fig. 12. Comparison of sizing results: UDDS vs. WLTP drive cycle.

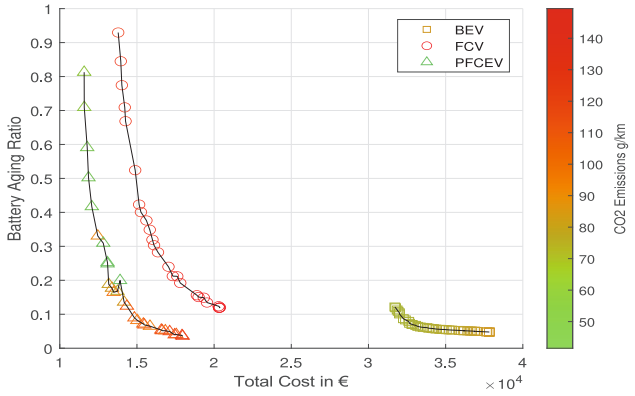

Fig. 13. Comparative Pareto Fronts for PFCEV, FCV and BEV.

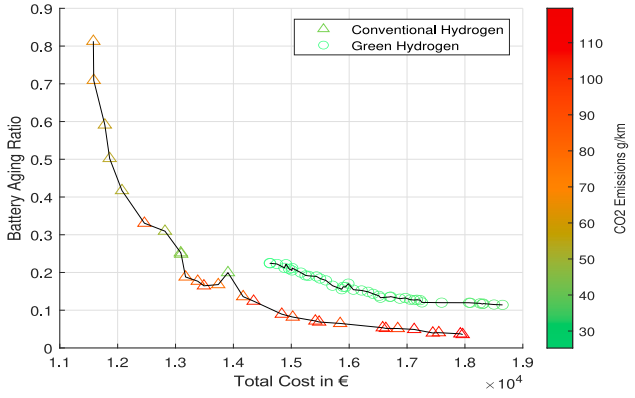

Fig. 14. Comparative Pareto Fronts for PFCEVs: Conventional hydrogen vs. Green hydrogen.

by temperature. Furthermore, we will integrate a real-time EMS that may necessitate vehicle trajectory prediction or planning to effectively distribute power among sources in real time, with the goal of minimizing both driving costs and component aging. Future directions for designing EMS should incorporate thermal management strategies. It is anticipated that these advancements will enhance the efficiency and service life of fuel cell hybrid electric vehicles when compared to energy management strategies that do not consider temperature effects. Additionally, the project aims to experimentally validate the algorithm's performance using the IREENA Lab "Smart Power" test bench.

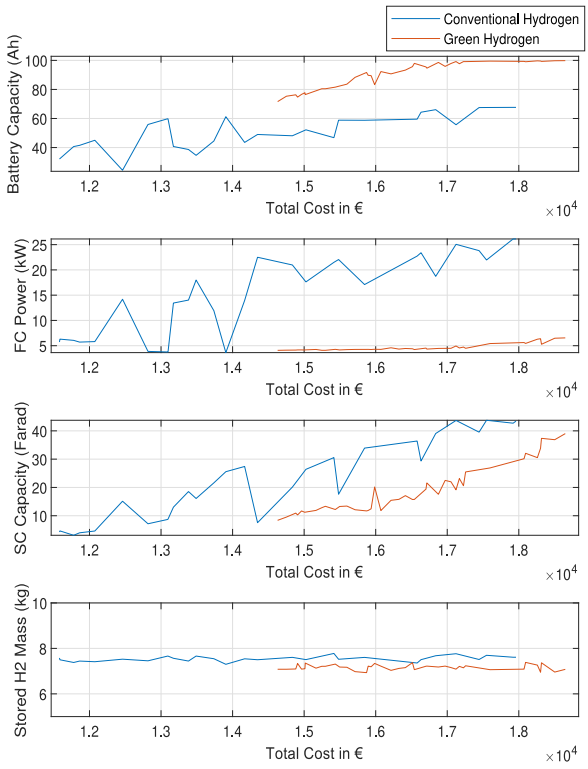

Fig. 15. Sizing result for the PFCEVs: Conventional hydrogen vs. Green hydrogen.

CRediT authorship contribution statement

Ahmad Eid El-Iali: Writing – review & editing, Writing – original draft, Validation, Software, Resources, Methodology, Conceptualization. **Moustapha Doumiati:** Writing – review & editing, Validation, Supervision, Project administration, Methodology, Investigation, Funding acquisition. **Mohamed Machmoum:** Supervision, Project administration, Methodology, Funding acquisition.

Declaration of competing interest

The authors declare that they have no known competing financial interests or personal relationships that could have appeared to influence the work reported in this paper.

Data availability

Data will be made available on request.

Acknowledgments

This work is carried out within the framework of the V3EA project "Electric, Energy Efficient and Autonomous Vehicle" (2021–2025), funded by the Research National Agency (ANR) of the French government.

References

[1] IEA, Global energy-related CO2 emissions by sector, 2020, 2020, https://www.iea.org/data-and-statistics/charts/global-energy-related-co2-emissions-by-sector-2020.

[2] Rabee Jibrin, Stuart Hillmansen, Clive Roberts, Convex optimization for fuel cell hybrid trains: Speed, energy management system, and battery thermals, in: 2022 European Control Conference, ECC, 2022, pp. 2130–2136.

[3] Qian Xun, Yujing Liu, Hengzhao Yang, Sizing and management of fuel cell based powertrains for city ferry applications, in: IECON 2022 – 48th Annual Conference of the IEEE Industrial Electronics Society, 2022, pp. 1–6.

[4] Stefan Kazula, Stefanie de Graaf, Lars Enghardt, Review of fuel cell technologies and evaluation of their potential and challenges for electrified propulsion systems in commercial aviation, J. Glob. Power Propuls. Soc. 7 (2023) 43–57.

[5] Michele Sparano, Marco Sorrentino, Giovanni Troiano, Giovanni Cerino, Giuseppe Piscopo, Marco Basaglia, Cesare Pianese, The future technological potential of hydrogen fuel cell systems for aviation and preliminary co-design of a hybrid regional aircraft powertrain through a mathematical tool, Energy Convers. Manage. 281 (2023) 116822.

[6] Eytan J. Adler, Joaquim R.R.A. Martins, Hydrogen-powered aircraft: Fundamental concepts, key technologies, and environmental impacts, Prog. Aerosp. Sci. 141 (2023) 100922, Special Issue on Green Aviation.

[7] M. Bai, W. Yang, J. Li, M. Kosuda, L. Fozo, M. Kelemen, Sizing methodology and energy management of an air–ground aircraft with turbo-electric hybrid propulsion system, Aerospace 9 (12) (2022) 764.

[8] Lei Zhang, Xiaosong Hu, Zhenpo Wang, Fengchun Sun, Junjun Deng, David. G. Dorrell, Multiobjective optimal sizing of hybrid energy storage system for electric vehicles, IEEE Trans. Veh. Technol. 67 (2) (2018) 1027–1035.

[9] Jiahao Huang, Zhiwu Huang, Yue Wu, Yongjie Liu, Heng Li, Fu Jiang, Jun Peng, Sizing optimization research considering mass effect of hybrid energy storage system in electric vehicles, J. Energy Storage 48 (2022) 103892.

[10] X. Zhang, C.C. Mi, A. Masrur, D. Daniszewsk, Wavelet-transform-based power management of hybrid vehicles with multiple on-board energy sources including fuel cell, battery and ultracapacitor, J. Power Sources 185 (2) (2008) 1533–1543.

[11] Giacomo Previati, Giampiero Mastinu, Matteo Gobbi, Thermal management of electrified vehicles—A review, Energies 15 (4) (2022) 1326.

[12] Sajjad Kharabati, Seyfolah Saedodin, A systematic review of thermal management techniques for electric vehicle batteries, J. Energy Storage 75 (2024) 109586.

[13] Daniel Watzenig, Bernhard Brandstätter, Comprehensive energy management - safe adaptation, predictive control and thermal management, in: SpringerBriefs in Applied Sciences and Technology, Springer Cham, 2018.

[14] G. Previati, G. Mastinu, M. Gobbi, Thermal management of electrified vehicles—A review, Energies 15 (4) (2022) 1326.

[15] Camilo Andrés Manrique-Escobar, Michele Sparano, Marco Sorrentino, Fuel cell plug-in hybrid electric vehicle thermal management strategy in parking time for low-temperature environments, J. Energy Storage 56 (2022) 106020.

[16] Z.S. Gelmanova, G.G. Zhabalova, G.A. Sivyakova, O.N. Lelikova, O.N. Onishchenko, A.A. Smailova, S.N. Kamarova, Electric cars. Advantages and disadvantages, J. Phys. Conf. Ser. 1015 (5) (2018) 052029.

[17] Nadia Asim, Adnan Bimani, Ahmed Al Saqri, Maria Matriano, The social and environmental impact of hybrid cars, Int. J. Res. Entrep. Bus. Stud. 1 (2020) 36–47.

[18] Meiling Yue, Hugo Lambert, Elodie Pahon, Robin Roche, Samir Jemei, Daniel Hissel, Hydrogen energy systems: A critical review of technologies, applications, trends and challenges, Renew. Sustain. Energy Rev. 146 (2021) 111180.

[19] Xueqin Lü, Siwei Li, XiangHuan He, Chengzhi Xie, Songjie He, Yuzhe Xu, Jian Fang, Min Zhang, Xingwu Yang, Hybrid electric vehicles: A review of energy management strategies based on model predictive control, J. Energy Storage 56 (2022) 106112.

[20] Bakou Traoré, Moustapha Doumiati, Jean-Christophe Olivier, Cristina Morel, Adaptive power sharing algorithm combined with robust control for a multi-source electric vehicle: Experimental validation, Int. Rev. Electr. Eng. 17 (1) (2022) http://dx.doi.org/10.15866/iree.v17i1.21269.

[21] Eda Alpaslan, Sera Ayten Çetinkaya, Ceren Yüksel Alpaydın, S. Aykut Korkmaz, Mustafa Umut Karaoğlan, C. Ozgur Colpan, K. Emrah Erginer, Aytaç Gören, A review on fuel cell electric vehicle powertrain modeling and simulation, Energy Sources A (2021) 1–37.

[22] Huan Chen, Rui Xiong, Cheng Lin, Weixiang Shen, Model predictive control based real-time energy management for hybrid energy storage system, CSEE J. Power Energy Syst. 7 (4) (2021) 862–874.

[23] J. Moreno, M.E. Ortuzar, J.W. Dixon, Energy-management system for a hybrid electric vehicle, using ultracapacitors and neural networks, IEEE Trans. Ind. Electron. 53 (2) (2006) 614–623.

[24] V. Mounica, Y.P. Obulesu, An energy management scheme for improving the fuel economy of a fuel cell/battery/supercapacitor-based hybrid electric vehicle using the coyote optimization algorithm (COA), Front. Energy Res. 11 (2023) 1180531.

[25] Xiaosong Hu, Jie Han, Xiaolin Tang, Xianke Lin, Powertrain design and control in electrified vehicles: A critical review, IEEE Trans. Transp. Electr. 7 (3) (2021) 1990–2009.

[26] Yanjun Huang, Hong Wang, Amir Khajepour, Bin Li, Jie Ji, Kegang Zhao, Chuan Hu, A review of power management strategies and component sizing methods for hybrid vehicles, Renew. Sustain. Energy Rev. 96 (2018) 132–144.

[27] Liangfei Xu, Minggao Ouyang, Jianqiu Li, Fuyuan Yang, Languang Lu, Jianfeng Hua, Optimal sizing of plug-in fuel cell electric vehicles using models of vehicle performance and system cost, Appl. Energy 103 (2013) 477–487.

[28] E. Tazelaar, Y. Shen, P.A. Veenhuizen, T. Hofman, P.P. J. van den Bosch, Sizing stack and battery of a fuel cell hybrid distribution truck, Oil Gas Sci. Technol. 67 (4) (2012) 563–573.

[29] Tom Fletcher, Rob Thring, Martin Watkinson, An energy management strategy to concurrently optimise fuel consumption & PEM fuel cell lifetime in a hybrid vehicle, Int. J. Hydrog. Energy 41 (46) (2016) 21503–21515.
[30] Yonggang Liu, Jie Li, Zheng Chen, Datong Qin, Yi Zhang, Research on a multi-objective hierarchical prediction energy management strategy for range extended fuel cell vehicles, J. Power Sources 429 (2019) 55–66.
[31] Jiageng Ruan, Bin Zhang, Bendong Liu, Shuo Wang, The multi-objective optimization of cost, energy consumption and battery degradation for fuel cell-battery hybrid electric vehicle, in: 2021 11th International Conference on Power, Energy and Electrical Engineering, CPEEE, 2021, pp. 50–55.
[32] G. Kakoulaki, I. Kougias, N. Taylor, F. Dolci, J. Moya, A. Jäger-Waldau, Green hydrogen in Europe – a regional assessment: Substituting existing production with electrolysis powered by renewables, Energy Convers. Manage. 228 (2021) 113649.
[33] Amela Ajanovic, Mitchell Sayer, Reinhard Haas, The economics and the environmental benignity of different colors of hydrogen, Int. J. Hydrog. Energy 47 (57) (2022) 24136–24154.
[34] Mohamed Mroueh, Sarah Kassir, Moustapha Doumiati, Clovis Francis, Mohamed Machmoum, A new time scale based energy management strategy for a hybrid energy storage system in electrical microgrids, in: IECON 2021 – 47th Annual Conference of the IEEE Industrial Electronics Society, 2021, pp. 1–6.
[35] Fouad Boutros, Moustapha Doumiati, Jean-Christophe Olivier, Imad Mougharbel, Hadi Kanaan, New modelling approach for the optimal sizing of an islanded microgrid considering economic and environmental challenges, Energy Convers. Manage. 277 (2023) 116636.
[36] A combined optimization of the sizing and the energy management of an industrial multi-energy microgrid: Application to a harbour area, Energy Convers. Manage. 12 (2021) 100107.
[37] Protean Electric, PD18 in-wheel electric motor datasheet, 2018, [Online]. Available: https://www.proteanelectric.com/f/2018/05/Pd18-Datasheet-Master.pdf.
[38] F. Tarhini, R. Talj, M. Doumiati, Driving towards energy efficiency: A novel torque allocation strategy for in-wheel electric vehicles, in: IEEE 26th International Conference on Intelligent Transportation Systems, ITSC, Bilbao, Spain, 2023.
[39] Sarah Kassir, Moustapha Doumiati, Mohamed Machmoum, Francis Clovis, Maher El Rafei, Energy management system based on cost optimization of battery aging and hydrogen consumption in a microgrid, Int. Rev. Electr. Eng. 17 (2022) 346.
[40] Maitane Berecibar, Floris Devriendt, Matthieu Dubarry, Igor Villarreal, Noshin Omar, Wouter Verbeke, Joeri Van Mierlo, Online state of health estimation on NMC cells based on predictive analytics, J. Power Sources 320 (2016) 239–250.
[41] Dong Hao, Jianping Shen, Yongping Hou, Yi Zhou, Hong Wang, An improved empirical fuel cell polarization curve model based on review analysis, Int. J. Chem. Eng. 2016 (2016) 1–12.
[42] Michael Nöst, Christian Doppler, Manfred Klell, Alexander Trattner, Thermal management of PEM fuel cells in electric vehicles, in: Comprehensive Energy Management - Safe Adaptation, Predictive Control and Thermal Management, Springer, 2017.
[43] Huicui Chen, Pucheng Pei, Mancun Song, Lifetime prediction and the economic lifetime of proton exchange membrane fuel cells, Appl. Energy 142 (2015) 154–163.
[44] Pucheng Pei, Qianfei Chang, Tian Tang, A quick evaluating method for automotive fuel cell lifetime, Int. J. Hydrog. Energy 33 (14) (2008) 3829–3836.
[45] Paul Kreczanik, Pascal Venet, Alaa Hijazi, Clerc Guy, Study of supercapacitor aging and lifetime estimation according to voltage, temperature, and RMS current, IEEE Trans. Ind. Electron. 61 (2014) 4895–4902.
[46] W. Chen, H. Xiao, Q. Wang, L. Zhao, M. Zhu, Integrated Vehicle Dynamics and Control, Wiley, Hoboken, 2016.
[47] U.S. Environmental Protection Agency, Fuel economy and EV range testing, 2021, https://www.epa.gov/greenvehicles/fuel-economy-and-ev-range-testing.
[48] Lei Zhang, David G. Dorrell, Genetic algorithm based optimal component sizing for an electric vehicle, in: IECON 2013 - 39th Annual Conference of the IEEE Industrial Electronics Society, 2013, pp. 7331–7336.
[49] R. Matousek, Genetic algorithm and advanced tournament selection concept, in: Nature Inspired Cooperative Strategies Optimization, vol. 236, 2009, pp. 189–196.
[50] Yavuz Eren, Haluk Gorgun, An applied methodology for multi-objective optimum sizing of hybrid electric vehicle components, Int. J. Hydrog. Energy 40 (5) (2015) 2312–2319.
[51] Clean Energy Institute, Battery technology, 2020, [Online]. Available: https://www.cei.washington.edu/education/science-of-solar/battery-technology/.
[52] Takashi Toya Keiichi Okajima, Masao Sudoh, Evaluation of CO2 emission on supercapacitor system as energy storage device for hybrid electric vehicle. Department of Materials Science and Chemical Engineering, Shizuoka University 3-5-1 Johoku, Hamamatsu, Shizuoka 432-8561, Japan.
[53] BloombergNEF, Lithium-ion battery pack prices rise for first time to an average of $151/kWh, 2022, [Online]. Available: https://about.bnef.com/blog/lithium-ion-battery-pack-prices-rise-for-first-time-to-an-average-of-151-kwh/.
[54] J. Pucker-Singer, C. Aichberger, J. Zupančič, C. Neumann, D.N. Bird, G. Jungmeier, A. Gubina, A. Tuerk, Greenhouse gas emissions of stationary battery installations in two renewable energy projects, Sustainability 13 (11) (2021) 6330.
[55] globalpetrolprices, France electricity prices, 2023, [Online]. Available: https://www.globalpetrolprices.com/France/electricity_prices/.
[56] Statista, Carbon intensity of the power sector in France from 2000 to 2021, 2023, [Online]. Available: https://www.statista.com/statistics/1290216/carbon-intensity-power-sector-france/.
[57] Hossein Pourrahmani, Adel Yavarinasab, Majid Siavashi, Mardit Matian, Jan Van herle, Progress in the proton exchange membrane fuel cells (PEMFCs) water/thermal management: From theory to the current challenges and real-time fault diagnosis methods, Energy Reviews 1 (1) (2022) 100002.
[58] Shankar Dhanushkodi, Nader Mahinpey, Asha Srinivasan, M. Wilson, Life cycle analysis of fuel cell technology, J. Environ. Informat. 11 (2008).
[59] Horizon Europe, Advanced materials for hydrogen storage tanks, 2023, [Online]. Available: https://www.horizon-europe.gouv.fr/advanced-materials-hydrogen-storage-tanks-34822.
[60] InnoEnergy Scandinavia, Unlocking new possibilities through innovative energy storage the role of ultracapacitors in the energy transition, 2020, [Online]. Available: https://eit.europa.eu/sites/default/files/white_paper_on_ultracapacitor_technology.pdf.
[61] Kiane de Kleijne, Heleen de Coninck, Rosalie van Zelm, Mark A.J. Huijbregts, Steef V. Hanssen, The many greenhouse gas footprints of green hydrogen, Sustain. Energy Fuels R. Soc. Chem. 6 (19) (2022) 4383–4387.
[62] A. Ajanovic, M. Sayer, R. Haas, The economics and the environmental benignity of different colors of hydrogen, Int. J. Hydrog. Energy 47 (57) (2022) 24136–24154, Hydrogen Society.